Full Title: Simulated hemiparesis increases optimal spatiotemporal gait asymmetry but not metabolic cost

Short Title: Spatiotemporal gait asymmetries with simulated hemiparesis

Russell T. Johnson[1], Nicholas A. Bianco[2], James M. Finley[1,3,4]

Affiliations:

1. Division of Biokinesiology and Physical Therapy, University of Southern California, Los Angeles CA, USA
2. Department of Mechanical Engineering, Stanford University, Palo Alto CA, USA
3. Department of Biomedical Engineering, University of Southern California, Los Angeles CA, USA
4. Neuroscience Graduate Program, University of Southern California, Los Angeles CA, USA

Corresponding Author: Russell T. Johnson, rtjohnso@usc.edu

Key Words: Post-stroke, Muscle Strength, Musculoskeletal modeling, Optimal control, Locomotion

Abstract

Several neuromuscular impairments, such as weakness (hemiparesis), occur after an individual has a stroke, and these impairments primarily affect one side of the body more than the other. Predictive musculoskeletal modeling presents an opportunity to investigate how a specific impairment affects gait performance post-stroke. Therefore, our aim was to use to predictive simulation to quantify the spatiotemporal asymmetries and changes to metabolic cost that emerge when muscle strength is unilaterally reduced. We also determined how forced spatiotemporal symmetry affects metabolic cost. We modified a 2-D musculoskeletal model by uniformly reducing the peak isometric muscle force in all left-limb muscles. We then solved optimal control simulations of walking across a range of speeds by minimizing the sum of the cubed muscle excitations across all muscles. Lastly, we ran additional optimizations to test if reducing spatiotemporal asymmetry would result in an increase in metabolic cost. Our results showed that the magnitude and direction of effort-optimal spatiotemporal asymmetries depends on both the gait speed and level of weakness. Also, the optimal metabolic cost of transport was 1.25 m/s for the symmetrical and 20% weakness models but slower (1.00 m/s) for the 40% and 60% weakness models, suggesting that hemiparesis can account for a portion of the slower gait speed seen in people post-stroke. Adding spatiotemporal asymmetry to the cost function resulted in small increases (~4%) in metabolic cost. Overall, our results indicate that spatiotemporal asymmetry may be optimal for people post-stroke, who have asymmetrical neuromuscular impairments. Additionally, the effect of speed and level of weakness on spatiotemporal asymmetry may explain the well-known heterogenous distribution of spatiotemporal asymmetries observed in the clinic. Future work could extend our results by testing the effects of other impairments on optimal gait strategies, and therefore build a more comprehensive understanding of the gait patterns in people post-stroke.

Author Summary

A stroke causes damage to the brain. This typically results in several changes to the nervous and muscular (neuromuscular) system that change how people post-stroke tend to walk and perform other tasks. Individuals post-stroke tend to walk with an asymmetrical motion and expend more energy while walking than other age-matched individuals. We still do not understand how each specific change to the neuromuscular system is linked with changes in walking patterns, in part because it is difficult to test one individual change at a time in people. Instead, we can use a mathematical model of the musculoskeletal system that represents the individual changes to the muscular system that occur in people post-stroke. In this study, we modeled how a common change in people post-stroke (muscle weakness) can impact walking patterns. We found that the level of weakness and the walking speed affect the asymmetrical walking patterns of our models, but do not change the total energy cost. Overall, our study is one step towards better understanding how neuromuscular changes in people post-stroke affects walking patterns. This knowledge could be applied to identify rehabilitation strategies that are most likely to improve walking in people post-stroke.

1. Introduction

Many neuromuscular impairments occur after an individual has a stroke (1–3), such as muscle spasticity (4,5), reductions in muscle strength (6,7), and generation of abnormal patterns of muscle coordination (8–10). These changes often preferentially affect the side of the body that is contralateral to the side of the neural damage. The lateralized neuromuscular impairments result in marked gait deviations: people post-stroke walk slower, spend more time in double support, and typically display asymmetrical step lengths, step times, and joint kinematics (11–13). In addition to slower preferred gait speeds and spatiotemporal asymmetries, people post-stroke also walk with a greater metabolic cost of transport (COT) than age- and speed-matched control subjects (11,14). An ongoing objective for clinicians and researchers is to determine the causal associations relating neuromuscular impairments, gait deviations, and the energetic cost of walking (11,15–18). This knowledge could potentially be used to identify intervention targets that are most likely to improve rehabilitation outcomes.

Determining causal links between neuromuscular impairments and gait performance is challenging because it is currently impossible to independently modulate all known impairments in people post-stroke and then observe the effects of these changes on gait deviations or metabolic cost. Instead, some researchers have investigated the effects of select gait deviations on metabolic energy cost. When neurotypical individuals walk with increased spatiotemporal asymmetries, their metabolic COT increases compared to symmetrical walking patterns (19,20). As such, some common rehabilitation interventions have targeted these spatiotemporal asymmetries to try to improve outcome measures of gait performance in people post-stroke. However, recent studies using biofeedback have shown little or no improvement in metabolic COT when people post-stroke walk with more symmetric step lengths (21–25). Therefore, it is still unclear how impairment interacts with observable gait deviations to cause the increase in metabolic COT in this population.

Musculoskeletal modeling and predictive simulation provide the opportunity to generate predictions about how specific neuromuscular impairments affect gait performance as researchers can

modify muscle parameters in a systematic way while keeping other parameters unchanged (26,27). Previous researchers have used musculoskeletal modeling and predictive simulation to predict gait patterns for both healthy and clinical populations, such as people with cerebral palsy or people who walk with lower limb prosthetics (26,28–30). This approach has led to valuable insight into principles of motor control (28,31,32), the effect of impairments on gait mechanics and energetics (26,27,33,34), and the effect of gait patterns on joint loading (35,36). Overall, these studies, along with recent advancements in both computational efficiency and accessibility (37–39), have allowed predictive modeling and simulation studies to help reveal important principles of gait mechanics (40). Therefore, we can apply the methodology of musculoskeletal modeling and predictive simulation to understand the optimal gait patterns for people with neuromuscular impairments.

The aim of this study was to use predictive simulations to explore how a common impairment in people post-stroke, hemiparesis, should impact patterns of spatiotemporal asymmetry and metabolic cost for gait patterns that minimize muscular effort. Hemiparesis is defined as a decrease in muscular strength that primarily affects one side of the body, the effects of which are distinct from other associated post-stroke impairments like abnormal co-activation across muscles or muscle spasticity. To simulate hemiparesis in our musculoskeletal model, we systematically reduced the peak isometric muscle strength for all the muscles on the left limb of our model while keeping the right limb constant and evaluated patterns of spatiotemporal asymmetry and metabolic cost that emerged across a wide range of speeds while minimizing muscle excitations. We hypothesized that asymmetric walking patterns would emerge as being optimal as we increased the magnitude of unilateral weakness. We then asked how enforcing symmetric step lengths and step times in models with unilateral weakness impacted the metabolic cost of transport. Here, we expected that enforcing symmetry would lead to marked increases in the metabolic cost of transport when compared to models where symmetry was not enforced. Overall, this work will allow us to gain insight into how muscle strength impairments impact gait deviations and the metabolic energy cost of walking, independent of other neuromuscular changes that occur post-stroke.

2. Methods

2.1 Musculoskeletal Model:

A two-dimensional, sagittal-plane musculoskeletal model with 11 degrees-of-freedom (DOF) was used (Fig 1A) within the OpenSim Moco software to generate optimal control simulations of walking (37). The model had a pelvis that translated and rotated relative to the ground with 3 DOF and the torso was rigidly attached to the pelvis. Each hip, knee, ankle, and toe joints were each modeled as 1 DOF pin joints. The model was actuated with 24 Hill-type muscle-tendon units (12 per limb) based on the *DeGrooteFregly2016Muscle* model with compliant series elastic elements (41). The foot-ground interactions were simulated using five contact spheres per foot, represented with smooth and continuous functions (42). We used this musculoskeletal model with symmetrical strength for the base conditions, and then created three other models where the peak isometric strength of each muscle on the left limb was reduced from the base model by 20%, 40%, and 60% for the three hemiparetic conditions (Fig 1B; Table 1). This unilateral reduction in peak strength was intended to simulate the loss of force production capacity that commonly results from stroke. Although the weakness resulting from acute stroke results from a loss of descending drive from the brain, we would need to simulate large reductions in feasible excitations for this loss to impact the patterns of muscle activation observed in a sub-maximal task like walking. In addition, because the magnitude of a given loss of descending drive to a set of muscles is less practical to measure empirically than the resulting weakness, therefore this approach can be more easily extended to personalize predictive simulations.

Table 1: Peak isometric strength (in N) for each of the 12 muscles for each model. The right limb strength remained unchanged (Base values) while the left limb strength was modified for the 20%, 40%, and 60% weakness models.

	Symmetrical	20%	40%	60%
Biceps long head	4105	3284	2463	1642
Biceps short head	557	445.6	334.2	222.8
Gluteus maximus	4450	3560	2670	1780
Psoas	2448	1958.4	1468.8	979.2
Rectus femoris	2192	1753.6	1315.2	876.8
Vastus Intermedius	9593	7674.4	5755.8	3837.2
Gastrocnemius	4691	3752.8	2814.6	1876.4
Soleus	6194	4955.2	3716.4	2477.6
Tibialis anterior	1227	981.6	736.2	490.8
Extensor hallucis longus	889	711.2	533.4	355.6
Flexor digitorum longus	1331	1064.8	798.6	532.4
Flexor digitorum brevis	938	750.4	562.8	375.2

2.2 Optimal Control Problem for Nominal Conditions

We ran several sets of optimal control problems in Moco, which were solved by minimizing the sum of the integrated muscle excitations cubed divided by the horizontal displacement of the center of mass (Eq. 1), which is hypothesized to represent minimizing muscle fatigue (28,43). While it is unclear what objective function best explains features of human gait, several studies have suggested that humans select gait patterns that reduce the muscular effort, muscle fatigue, or metabolic energy associated with the task (44–49). These studies provide evidence that effort optimization may explain why we choose certain spatiotemporal features of our gait during steady-state walking and when exposed to novel task demands.

Direct collocation was used to solve for the set of states and controls needed to produce a full gait cycle, subject to the objective function and constraints. The set of states, x, were 11 generalized coordinates $q(t)$ corresponding to each joint and the three degrees of freedom for the pelvis, 11 generalized velocities $u(t)$, 24 muscle activations $a(t)$, and 24 normalized tendon forces $\widetilde{F^T}(t)$. The set of controls consisted of 24 muscle excitations $e(t)$ and 24 auxiliary variables representing the derivative of normalized tendon force $\dot{\widetilde{F^T}}(t)$, which were necessary for enforcing the muscle-tendon equilibrium equations in implicit form (Eq. 2; 41). The states and controls were discretized on a grid of 201 evenly distributed nodes over a complete gait cycle. Optimal control problems were solved for each of the four models for speeds of 0.25, 0.50, 0.75,

136 1.00, and 1.25 m/s. Each problem was formulated to generate a full stride of walking by finding the set of
137 model states, controls, and final time t_f, subject to the objective function (Eq. 1),

$$J_1 = \frac{\sum_{i=1}^{24} \int_0^{t_f} e_i^3(t)\, dt}{q_{pelvis_x}(t_f) - q_{pelvis_x}(0)} \tag{1}$$

138 where e_i is the excitation of the ith muscle and q_{pelvis_x} is the horizontal position of the pelvis such that the
139 denominator represents the displacement of the model during the gait cycle.

140 Each optimal control problem was solved by minimizing J_1 subject to constraints enforcing skeletal
141 kinematics, skeletal dynamics, muscle activation dynamics, and implicit tendon compliance dynamics (Eq.
142 2; 37,41),

$$\begin{gathered} u(t) = \dot{q}(t) \\ \dot{u}(t) = f\left(q(t), u(t), a(t), \widetilde{F^T}(t)\right) \\ \dot{a}(t) = f\left(e(t), a(t)\right) \\ f\left(a(t), \widetilde{F^T}(t), \dot{\widetilde{F^T}}(t)\right) = 0 \end{gathered} \tag{2}$$

143 Bounds were placed on the states, controls, and auxiliary variables (Eq. 3).

$$\begin{gathered} q_{LB}(t) \le q(t) \le q_{UB}(t) \\ u_{LB}(t) \le u(t) \le u_{UB}(t) \\ 0.001 \le e(t) \le 1 \\ 0.001 \le a(t) \le 1 \\ 0 \le \widetilde{F^T}(t) \le 1.8 \\ -1000 \le \dot{\widetilde{F^T}}(t) \le 1000 \end{gathered} \tag{3}$$

144 where q_{LB}, q_{UB}, u_{LB} and u_{UB} represent the lower and upper bounds on each kinematic value and speed,
145 respectively. Excitations $(e(t))$ and activations $(a(t))$ were bounded between 0.001 and 1. Normalized
146 tendon forces $(\widetilde{F^T}(t))$ were bounded between 0 and 1.8 and their derivative $(\dot{\widetilde{F^T}}(t))$ were bounded between

-1000 and 1000. Lastly, the optimization was also subject to periodicity constraints, where the final states and controls must equal the initial states and controls, except for the horizontal position of the pelvis $q_{pelx}(t)$, which must account for horizontal translation relative to the target velocity v and t_f (Eq. 4).

$$\begin{aligned} q(t_f) &= q(0) \\ q_{pelvis_x}(t_f) &= q_{pelvis_x}(0) + (v * t_f) \\ u(t_f) &= u(0) \\ e(t_f) &= e(0) \\ a(t_f) &= a(0) \\ \widetilde{F^T}(t_f) &= \widetilde{F^T}(0) \end{aligned} \tag{4}$$

The final time of the gait cycle was allowed to vary within the optimization between 0.3 and 2 seconds, which allowed the optimization to use the optimal stride length and stride time which satisfied the target gait speed for each condition (Fig 1C).

We used three different initial guesses for each of the 20 conditions (four models and five speeds each). The first initial guess was the result of a tracking optimization which used averaged gait data from healthy control subjects walking at 1.4 m/s (31). The reference data were normalized to 101 time points to align the data with the collocation points of the optimizations. The first initial guesses for each speed were generated by minimizing a weighted combination of the total integrated muscle excitations cubed and the difference between experimental and simulated kinematics and ground reaction forces (Eq. 5), while matching the average gait speed (i.e., 0.25, 0.50, 0.75, 1.00, and 1.25).

$$J_{track} = J_1 + \int_0^{t_f} \left[\left(w_1 * \sum_{i=1}^{11} \left(\frac{q_i(t) - \widehat{q_i}(t)}{\sigma_{qi}} \right)^2 + \left(\frac{u_i(t) - \widehat{u_i}(t)}{\sigma_{ui}} \right)^2 \right) + \left(w_2 * \sum_{j=1}^{4} \left(\frac{GRF_j(t) - \widehat{GRF_j}(t)}{\sigma_j} \right)^2 \right) \right] dt \tag{5}$$

For Equation 5, the term J_1 represents the muscular effort (Eq. 1). The second and third terms represent deviations from the experimental kinematics and ground reaction forces (GRFs), respectively. $q_i(t)$ and $u_i(t)$ are the values and velocities of model coordinate i at time t, $\widehat{q_i}(t)$ and $\widehat{u_i}(t)$ are the reference

kinematic data from Miller (2014) of coordinate *i* at time *t*, and σ_{qi} and σ_{ui} are the standard deviations of the reference data, averaged across the stride. $GRF_j(t)$ represents the model ground reaction forces at time *t* for the horizontal and vertical forces for the left and right side, and $\widehat{GRF_j}(t)$ and σ_j represent the reference ground reaction force data means and standard deviations for each direction and limb. This initial guess was used for each of the four models for the corresponding walking speed (e.g., the tracking solution for 0.75 m/s was used as an initial guess for each of the four models at 0.75 m/s speed). While the reference data from Miller, 2014 was at a different gait speed than the speeds used in this study, the tracking problem solutions produced realistic gait mechanics across speeds and were reasonable initial guesses for our predictive simulations.

The other two initial guesses were chosen heuristically from solutions of other conditions, either for different speeds or for different simulated hemiparesis models. For example, the 20% weak model at 0.75 m/s had the following initial guesses: (1) tracking solution at a speed of 0.75, (2) the solution to the 20% weak model at 1.00 m/s, and (3) the 40% weak solution at 0.75 m/s. If the solutions differed between initial guesses, we chose the optimal solution for each condition with the lowest objective function value, and this solution was then used to calculate the spatiotemporal asymmetry and metabolic cost (see Section 2.4).

2.3 Step Time and Step Length Symmetry Conditions

Many of the optimal gait patterns observed for models of varying levels of weakness were spatiotemporally asymmetric. Since reducing these asymmetries is a common rehabilitation objective for people post-stroke (50), we conducted a second set of optimizations to determine how reducing the step length and step time asymmetry would impact metabolic cost. Therefore, we added two terms to the objective function (J_2; Eq. 6) that allowed us to reduce step time symmetry or step length symmetry for the different models.

$$J_2 = J_1 + \left(w_1 * SLA_{goal}\right) + \left(w_2 * STA_{goal}\right) \quad (6)$$

The step length symmetry goal (SLA_{goal}) was formulated to minimize the step length asymmetry (SLA; Eq. 7) during the stride. Theoretically, we would want to compute the step length for the non-paretic (SL_{NP}) and paretic (SL_P) sides across the gait cycle for each iteration. However, this approach does not work well for predictive simulations because gradient-based optimization approaches require smooth, differentiable objective function terms in order to achieve reliable convergence. Therefore, we instead approximated step length asymmetry by performing the following steps. We first set the total stride length to be equal to the stride length of the respective nominal condition (i.e., the stride length from the 0.75 m/s speed with 20% weakness), such that the stride length is matched within a speed/model condition. Then, to target a symmetrical step length, we computed the length for the right and left step that would both result in symmetrical step lengths during the gait cycle. To enforce these step lengths during the optimization, we set penalties that accumulate if distance between the feet exceed the targeted step length distance for each foot. Therefore, we are indirectly setting the step length for the paretic and non-paretic step using smoothing functions that work well for the optimization algorithm (see supporting information).

$$SLA = \frac{SL_{NP} - SL_P}{SL_{NP} + SL_P} \times 100 \tag{7}$$

The step time symmetry goal (STA_{goal}) was designed to reduce the step time asymmetry during the gait cycle (Eq. 8). As with the SLA_{goal}, we needed to find an approximate form of step time asymmetry for this goal to work well within our optimization framework. Therefore, for this goal, we computed an approximation of step time asymmetry by detecting the number of time points each foot was in contact with the ground and computed the asymmetry index by normalizing by the total number of time points. Time points when both feet were in contact were assigned to the leading foot. Once we have the total number of nodes for non-paretic (ST_{NP}) and paretic step time (ST_P), respectively, we can then compute the asymmetry index based on the number of nodes and the stride time (see supporting information).

$$STA = \frac{ST_{NP} - ST_P}{ST_{NP} + ST_P} \times 100 \tag{8}$$

Since each of these symmetry goals are approximations of step length and step time asymmetries, we then computed the actual asymmetry indices to check if the optimal solution achieves the intended symmetrical pattern. If there were large discrepancies, we would then be able to adjust settings on the SLA or STA goal and re-run the optimization. We chose to run this symmetry sub-analysis on the 0.75 m/s speed because the nominal results had a consistent pattern of increasing step length asymmetry with greater hemiparesis. First, we solved a new set of optimal control problems to reduce the step time symmetry for each model at 0.75 m/s. For the first set of optimizations, w_1 was set to 8 and w_2 was set to 0, such that reducing the step length asymmetry was part of the objective, but step time asymmetry.

Finally, we solved another set of optimal control problems at 0.75 m/s with the added goal of reducing both step length and step time asymmetry. In this case, the weighting for J_2 were set as w_1 set to 8 and w_2 set to 5. These weightings were chosen heuristically such that we were able to reduce the asymmetry in each domain while getting good convergence. We noticed that if either w_1 or w_2 were too large, the optimization would not converge in a reasonable amount of time.

2.4 Optimization Settings

All optimal control problems (28 total: four models x five speeds, plus four more for step time symmetry and four more for step length symmetry) were solved with 201 evenly spaced grid points, with Hermite-Sampson discretization (51), using CasADi (52) and IPOPT (53). Termination settings for the optimization were: 1e-4 constraint violation tolerance and 1e-4 convergence tolerance. Optimizations were solved on a four-core desktop computer with a 3.3 GHz Intel Core i5-6600 processor. In total, we ran 84 optimizations for the nominal conditions (28 conditions with 3 initial guesses each), plus 18 additional optimizations for the symmetrical goal conditions. Each of the individual optimizations was solved on our desktop computer in times ranging from 2 to 14 hours, depending on the condition and initial guess.

234 *2.5 Outcome Measures and Evaluations*

235 The step length for the non-paretic (right) limb was calculated by taking the anterior-posterior (AP)
236 distance between the ground-contact elements on the heels at the instant of non-paretic foot-strike where
237 foot-strike was defined as the point when the vertical GRF was greater than 20 N (54). The step length for
238 the paretic (left) limb was calculated similarly at the instant of paretic foot-strike. Step time for the non-
239 paretic limb was calculated as the time from paretic foot-strike to non-paretic foot strike, and step time for
240 the non-paretic limb was calculated as the time from non-paretic foot-strike to paretic foot-strike.

241 The metabolic cost of transport (COT) for each condition was also estimated based on the
242 *Umberger2010MuscleMetabolicsProbe* accessed through OpenSim (55,56). The COT was calculated for
243 each condition while holding muscle mass constant, to replicate weakness in the limb without muscle
244 atrophy. In addition to predicting the change in COT between conditions, the positive and negative muscle
245 fiber work performed for each muscle was also calculated (Eq 11), since muscle fiber work is a component
246 of the metabolic cost model. First, the muscle fiber power was calculated for each muscle across time, then
247 the positive and negative portions of the power curve were separately integrated to calculate positive and
248 negative mechanical work, respectively for each limb. For the non-paretic side, positive mechanical power
249 (W_{NP}^{+}) was calculated by:

$$W_{NP}^{+} = \sum_{m=1}^{12} \int_{0}^{t_f} P_{NP_m}^{+} \, dt \tag{11}$$

250

251 where m is each of the 12 muscles of the limb, t_f equals the total time of the stride and $P_{NP_m}^{+}$ is the positive
252 mechanical power for the mth muscle on the non-paretic side. Negative mechanical work was calculated
253 based on the negative power of each non-paretic muscle. The positive and negative mechanical work for
254 the paretic limb was calculated the same way as above, but with power data from the paretic limb. As with
255 the metabolic COT calculations, we normalized both the positive and negative mechanical work by dividing
256 by displacement to compute the positive and negative mechanical COT.

Lastly as different metabolic cost models can result in different predictions of metabolic cost (57), we evaluated whether our results would change with a different metabolic cost model. Therefore, we computed the metabolic COT using the Bhargava model (58) for each of the nominal conditions to compare with the results from the Umberger model.

3. Results

3.1 Overview and Model Validation

Overall, the kinematic and GRF results for the base model across speeds shared broad similarities in patterns with previous experimental data, which gave us confidence that the modeling and optimization methods we used produced sensible results. For example, peak knee flexion angle occurred earlier in the gait cycle as speed increased (Fig 2B), which aligns with experimental results (59). The peak ankle plantarflexion angle at push-off also occurred earlier in the gait cycle at faster speeds compared with slower speeds (Fig 2C), also matching with experimental data (59). Generally, the GRFs also matched experimental data, with greater peak vertical GRFs (Fig 2D) and greater posterior GRFs during early stance (Fig 2E) for faster speeds (60). Across all speeds, the step time and step length variables were each close to symmetrical for the base model, demonstrating that the optimal gait patterns for symmetrical models were symmetrical (Fig 3A and 3D).

3.2 Effects of Simulated Hemiparesis on Spatiotemporal Asymmetry

Generally, for models with muscle strength asymmetries, the optimal solution resulted in asymmetrical spatiotemporal patterns where the magnitude and direction of the asymmetries depended on both the level of muscle weakness and the gait speed (Fig 3A and 3B). For slower gait speeds (e.g., 0.25 and 0.50 m/s), the optimization resulted in a positive step time asymmetry for both the 40% and 60% weakness models which corresponds to the model taking longer to transition from the paretic to non-paretic limb than vice versa. At faster speeds (e.g., 1.00 or 1.25 m/s) the optimal gait pattern had a negative step

time asymmetry for those same models. This suggests that the direction of step time asymmetry (positive or negative) is impacted by the gait speed that an individual walks and the degree of muscle weakness. Generally, the step times for the non-paretic side (Fig 3B) were about 0.40 seconds across most speeds and conditions, while the step times for the paretic side (Fig 3C) across the conditions were greater at faster speeds than slower speeds (i.e., ~0.40 seconds at slower speeds and ~0.50 seconds at faster speeds).

The direction and magnitude of step length asymmetry also varied depending on both the level of muscle weakness and the gait speed (Fig 3D). Marked step length asymmetries were generally observed once strength was reduced by 40%. For most speeds, the optimal solution for the model with 40% weakness was a positive step length asymmetry, with the largest asymmetry being observed in the weakest model at the slowest speed. These positive step length asymmetries correspond to a gait pattern where longer steps are taken with the paretic limb than the non-paretic limb. An exception to this trend occurred in the 1.25 m/s condition which resulted in a negative step length asymmetry. The optimal solutions produced greater step lengths on both the non-paretic (Fig 3E) and paretic (Fig 3F) sides for faster speeds compared with slower speeds. The 40% weakness model at 1.25 m/s resulted in step times and step lengths that stood out from other similar conditions, with a much shorter right step time and shorter right and left step lengths than other similar conditions (i.e., 40% weakness at 1.00 m/s or 60% weakness at 1.25 m/s).

3.3 Metabolic and Mechanical Cost of Transport for Nominal Conditions

Despite the optimal solutions having marked spatiotemporal asymmetries, the computed metabolic COT was relatively consistent within speeds across different model weaknesses (Fig 4A). At speeds between 0.25 and 0.75 m/s, the metabolic COT was similar across all models, but there were subtle differences across the models in metabolic COT at 1.00 and 1.25 m/s. The metabolic COT was greater in the 40 and 60% weakness models than the symmetrical and 20% weakness models at 1.25 m/s, whereas at 1.00 m/s the pattern was the opposite. Gait speed had a substantial effect on the computed metabolic COT across the speeds we tested, with greater COT at slower gait speeds than faster gait speeds. At faster gait speeds (e.g., 1.00 and 1.25 m/s), the metabolic COT was between 3-4 J/kg/m, while at slower speeds (e.g.,

309 0.25 and 0.50) the metabolic COT was close to 10 J/kg/m, which matches closely with the trend of
310 metabolic COT across speeds in neurotypical individuals (11,47). The consistency of the COT for a given
311 speed resulted from complementary changes in limb-specific metabolic COT. Metabolic COT on the non-
312 paretic limb increased with greater weakness levels (Fig 4B) while COT was reduced proportionally on the
313 paretic limb (Fig 4C).

314 One important factor to consider when determining metabolic energy consumed by muscles is the
315 amount of mechanical work done by each muscle during walking (61,62). Therefore, we evaluated how
316 positive and negative mechanical work changed across speeds and conditions. Overall, the optimal solutions
317 resulted in gait patterns that had greater positive mechanical COT at slower gait speeds (Fig 4D).
318 Additionally, for models with greater muscle weakness there was a decrease in the magnitude of the positive
319 mechanical COT. While the non-paretic limb had a similar level of positive mechanical COT across the
320 different models within a speed (Fig 4F), the reduction in total positive mechanical work was driven by a
321 considerable decrease in the magnitude of positive mechanical COT by the paretic limb with increasing
322 weakness (Fig 4F). These trends were also seen for negative mechanical COT, with greater negative
323 mechanical COT at slower speeds and a decrease in negative mechanical COT with greater muscle
324 weakness.

325 The second important factor in determining metabolic energy consumed by muscles is the level of
326 muscle activation throughout the gait cycle. Total muscle activation increases at both faster gait speeds and
327 greater levels of simulated hemiparesis (Fig 4G). At the individual limb level, the muscle activations for
328 the non-paretic and paretic limbs increase with speed and weakness as well (Fig 4H and 4I). Overall, the
329 metabolic energy cost does not significantly vary across level of simulated hemiparesis, which is likely a
330 result of a decrease in mechanical muscle fiber work which offsets the increase in muscle activation with
331 greater muscle weakness.

332 We observed a typical U-shaped pattern of metabolic COT with respect to gait speed within a model
333 (Fig 5). Using these results, we can identify the “effort-optimal” solutions that resulted in the minimum
334 metabolic COT within a model across the speeds. For both the base and 20% weakness models, the

minimum metabolic COT occurred at a gait speed of 1.25 m/s, which is similar to what is observed experimentally in neurotypical individuals (47,63,64). For the 40% and 60% weakness models, the minimum metabolic COT instead occurred at a slower speed of 1.00 m/s.

To evaluate the sensitivity of our results and conclusions to the metabolic model chosen, we computed the metabolic COT using the Bhargava metabolic model (58). The Bhargava model resulted in slightly greater metabolic COT (average offset of 0.37 ± 0.17 J/kg/m) than the Umberger model, but the trends across the conditions were similar which suggests that our conclusions would not change with either the Umberger or Bhargava energetics models.

3.4 Effects of Minimizing Step Length and Step Time Asymmetry in a Model of Hemiparesis

Finally, we evaluated whether the predicted metabolic COT would change when enforcing step length or step time symmetry for models with simulated hemiparesis. To perform this analysis, we added a term to the objective function which produced gait patterns with approximately symmetrical step lengths across the different hemiparetic models at a speed of 0.75 m/s. The optimal solutions for the 20%, 40%, and 60% models had step length asymmetry indices less than 1.5%, which was close to the symmetrical target of 0% asymmetry (Fig 6B). However, this resulted in greater step time asymmetry for these gait patterns (Fig 6A). Minimizing step length symmetry resulted in a slightly greater metabolic COT than the nominal conditions by 1-4% (Fig 6C). We then added a third term to the objective function, which in combination with the others, resulted in gait patterns that had approximately symmetrical step lengths (maximum asymmetry = 2.6%; Fig 6B) and step times (maximum asymmetry = -1%; Fig 6A). Despite adopting a gait that was nearly symmetric overall, the metabolic COT for these conditions was less than 1% greater compared to when step length asymmetry was minimized alone, and only deviated by 5% from the nominal conditions.

4. Discussion

4.1 Overview of Key Results

The purpose of this study was to quantify the spatiotemporal asymmetries and changes to metabolic cost that emerge from effort-optimal predictions of gait with models of simulated hemiparesis across a wide range of speeds. Predicting the optimal gait pattern for models with simulated hemiparesis allows us to gain insight into the isolated effect of unilateral muscle weakness on gait asymmetry and metabolic COT. We found that the magnitude and direction of spatiotemporal asymmetry depended on the level of muscle weakness as well as the gait speed, with greater asymmetries corresponding to a greater level of muscle weakness. We then compared the metabolic COT across all optimal gait patterns to assess whether simulated hemiparesis and spatiotemporal asymmetries correspond with an increase in metabolic cost. We found that the predicted metabolic COT varied little with increasing levels of weakness, but scaled with speed as expected based on experimental data (e.g., 47). Finally, we evaluated whether enforcing step length or step time symmetry for the hemiparetic models would increase the metabolic COT. The metabolic COT only changed by a maximum difference of 5% between the nominal and symmetrical conditions. Overall, our results suggest that the spatiotemporal asymmetries seen in people post-stroke might be derived in part from optimal adaptations to underlying impairments such as hemiparesis. However, the presence of gait asymmetries does not necessarily contribute to the increase in metabolic cost that is observed relative neurotypical individuals.

Overall, a greater level of hemiparesis resulted in a more asymmetrical gait pattern in both step time and step length across all speeds, however the direction of the asymmetry depended on the gait speed. The 20% weakness model had step time asymmetries ranging from -5 to 2% and step length asymmetries ranging from -10 to 6%, while the 60% weakness models had step time asymmetries ranging from -20 to 10% and step length asymmetries ranging from -3 to 70%. This suggests that the effort-optimal gait patterns for individuals with mild unilateral strength deficits may be closer to symmetrical, compared to individuals

with much greater muscle strength impairments who may have effort-optimal gait patterns with greater spatiotemporal asymmetries.

We also found that metabolic COT is relatively consistent across levels of simulated hemiparesis. Metabolic cost is impacted by the level of muscle activation and the magnitude of mechanical work done throughout the movement. While muscle activation increased with greater levels of simulated hemiparesis, the positive and negative work performed by the muscle fibers decrease with greater levels of simulated hemiparesis. The decrease in work performed by the muscle fibers is driven by a decrease in work done by the paretic limb due to less muscle force generation. Overall, this effectively creates a trade-off between muscle activation and mechanical work, resulting in a similar level of metabolic cost across models within a gait speed.

There were substantial speed effects on both spatiotemporal asymmetry and metabolic cost. The magnitude and direction of step length asymmetry was also dependent upon the gait speed. For hemiparetic gait, a positive step length asymmetry indicates shorter steps with the paretic limb than the non-paretic limb. This pattern can be expected of a person post-stroke if they are unable to swing their paretic limb forward. Many of the effort-optimal gait patterns fall into this category of having positive step length asymmetry with a couple of exceptions at the 0.25 and 1.25 m/s conditions. For the 60% weak model, there were greater positive step length asymmetries at slower speeds than for faster speeds. The overall task demands for the slow speed may allow the model to take extremely short paretic side steps, while still matching the task speed. The heterogeneity and relative ranges of both positive and negative step length asymmetries largely mirrors what has been measured in previous experiments of people post-stroke (25,65,66).

Our results suggest that the direction of step time asymmetry depends on the gait speed rather than the level of hemiparesis. At 1.25 m/s speed, the effort-optimal gait patterns resulted in negative step time asymmetries across the three hemiparetic models, while for the 0.25 m/s speed, the effort optimal gait patterns result in positive step time asymmetries. Paretic step time here was defined as the time from non-paretic foot strike to paretic foot strike, so it contains the duration of the double support time with the

412 leading, non-paretic limb and the paretic side swing time. Therefore, a negative step time asymmetry
413 (greater paretic step time than non-paretic step time) would suggest that the model is using its non-paretic
414 limb for body weight support and propulsion for a greater period than the paretic limb, which is what one
415 might expect since weakness occurs in the paretic limb. In contrast, a positive step time asymmetry may be
416 beneficial at the slow speeds because the paretic swing limb may be less able to take advantage of passive
417 dynamics relative to what happens at faster speeds, resulting in a greater activation during swing phase to
418 swing the leg forward.
419
420 *4.2 Clinical Implications for Post-Stroke Rehabilitation*
421 The results from our simulation study have generated a couple of testable hypotheses. First, that
422 the direction of spatiotemporal asymmetries depends on the severity of hemiparesis and walking speed. We
423 know that spatiotemporal asymmetries, such as step length asymmetry, in people post-stroke are
424 heterogeneous, with some individuals having longer step lengths with their paretic limb than their non-
425 paretic and others having shorter step lengths with their paretic limb than non-paretic limb (25,66), however
426 what drives these responses remains unclear (65). Our results suggest that one of the driving factors of
427 asymmetry could be the level of hemiparesis.
428 Furthermore, the hypothesized relationship between severity of hemiparesis and the effort-optimal
429 gait patterns (i.e., direction and magnitude of spatiotemporal asymmetries) suggests that clinical
430 rehabilitation programs could be individually tailored based on measures of between-limb differences in
431 strength. Typical goals for gait rehabilitation programs for people post-stroke are to have the individuals
432 walk more symmetrically (50,67). However, it's still an open question whether this goal could be
433 considered the optimal way to walk for people post-stroke, with recent data suggesting that symmetrical
434 step lengths do not improve measures of metabolic COT (23,25) and result in other kinematic and kinetic
435 asymmetries (22). The results of our predictive simulations are consistent with these studies: when we
436 enforced step length symmetry for the 0.75 m/s speed, the resulting gait pattern had significant step time
437 asymmetry, with a small increase in metabolic COT. The experimental results in combination with our

simulated results are reasonable given the underlying anatomical system is asymmetric, therefore optimal gait patterns are also likely to be asymmetric. However, that the symmetry conditions resulted in only small increases in metabolic COT suggest that there could be multiple gait strategies for people post-stroke that result in similar consumption of metabolic energy, therefore, patients who prioritize a symmetrical appearance of gait may be able to perform their preferred gait pattern without a large penalty on their endurance.

Another important research question for gait in people post-stroke is what are the factors that contribute most to the slower gait speed observed in this population compared to age-matched controls (16,25,68,69)? Our data suggest that moderate levels of hemiparesis could contribute to the reduction in the energy optimal gait speed, as minimum metabolic COT occurred at 1.00 m/s for the 40% and 60% weakness models compared with a minimum at 1.25 m/s for the base and 20% weak models. However, this slight reduction in speed does not match the difference in preferred gait speed in people post-stroke relative to control (i.e., ~0.7 m/s; 25). So, while unilateral muscle weakness may partially contribute to the reduction in gait speed, other types of impairments such as spasticity and abnormal muscle co-activation patterns or different priorities during gait (e.g., balance and comfort) may have additional contributions.

Lastly, our data present another potential explanation (besides metabolic COT) for slower walking speed in people post-stroke: preferred gait speed for people post-stroke may also be impacted by an individual's desire to minimize observable spatiotemporal asymmetries. Our data suggest that moderate speeds of 0.50 and 0.75 m/s result in effort-optimal gait patterns with moderate levels of gait asymmetry (<10% asymmetry indices), while slower (0.25 m/s) or faster speeds (1.00 or 1.25 m/s) can result in levels of gait asymmetry greater than 10%. Therefore, we can hypothesize that people post-stroke may walk with slower gait speeds than would be optimal from a metabolic COT point of view because this allows them to maintain lower levels of gait asymmetry than would be necessary for faster/optimal COT speeds. Further explanation of the preferred gait patterns in people post-stroke could be explained by factors like balance or comfort, though how people post-stroke sense and perceive of these factors is an important question that needs to be addressed but is beyond the scope of this study.

4.3 Modeling Decisions and Limitations

Our results build upon several modeling choices that we made throughout the study, and as such, there are a few limitations to our project that should be considered in future research. First, we constrained our model to move only in the sagittal plane because our primary kinematic variables of interest for this project were step length and step time asymmetry, which are also in the sagittal plane, and we wanted to simulate several conditions (across speeds and across hemiparetic models) in a timely manner.

Additionally, we chose an objective function that minimizes the integrated sum of muscle excitations cubed across all muscles, which has been proposed to be a representation of minimizing muscle fatigue, or maximizing muscle endurance (28). This objective is formulated from experimental data that suggests the muscle force-endurance relationship is approximately cubic (43,70). While we evaluated the predicted metabolic COT from the results, we did not use metabolic COT in the objective function. Therefore, there could be different gait patterns that would further reduce the metabolic cost across each of the conditions. However, while different objective functions will result in different gait patterns from an optimal control solution (28,36,71), we believe that using our chosen objective function is appropriate for this study as fatigue is likely to be especially relevant for people with neuromuscular impairments.

Finally, the modeling of hemiparesis in our project involved several decisions. First, we decided to model hemiparesis instead of other impairments such as abnormal muscle coordination patterns or other changes in muscle properties because hemiparesis is straightforward to model by reducing peak muscle forces in the model. Future work should add other impairments, either on their own or in combination with hemiparesis, to better understand the independent or combinatory effects of the array of impairments after a stroke. Further, we decided to simulate hemiparesis by reducing the peak isometric muscle forces instead of modifying the maximum excitation values, which would relate to the decrease in central drive in people post-stroke. Modeling decreased central drive in a predictive simulation paradigm is impractical from a computational standpoint, as it would only affect the results when the maximum allowable excitation in the simulated weakness condition is exceeded in the base conditions. In gait, most muscles operate in a submaximal state, oftentimes far below full excitation. Therefore, setting a threshold excitation of 60% of

baseline, for example, would likely result in no changes to the gait strategy since none of the muscles surpassed 60% excitation level during the baseline stride. Furthermore, modeling decreased central drive is challenging from a physiological standpoint because it is difficult to assess the magnitude of impairment in central drive *in vivo*, instead, it's much simpler to measure muscle strength in the limbs using a dynamometer (e.g., 10). Therefore, our choice of reducing peak isometric muscle force as a representation of a reduction in the ability to produce force allowed for a reasonable way to model hemiparesis and is applicable since measuring the magnitude of impairment can be easily done in clinical settings. Another important modeling decision was to keep muscle mass constant across all hemiparetic models to simulate muscle weakness without muscle atrophy. Muscle mass is used for computing metabolic COT, because the metabolic energy consumed by muscles depends on activation levels and the volume of muscle activated (56). If we instead modeled muscle weakness alongside muscle atrophy, it would result in a reduction in metabolic cost for the hemiparetic models compared with our results due to a reduction in activated muscle mass.

4.4 Conclusion

In this study, we predicted the effort-optimal spatiotemporal patterns for gait with simulated hemiparetic musculoskeletal models. We found that the magnitude and direction of spatiotemporal asymmetry is affected by the level of hemiparesis and the gait speed, which may explain the well-known heterogenous distribution of spatiotemporal asymmetries observed in clinical data. However, the greater metabolic COT observed in people post-stroke compared to controls does not appear to be driven by hemiparesis, and instead may be driven by factors like muscle co-activation or abnormal muscle synergy patterns. Further, our data predict that hemiparesis is one aspect that could lead to slower self-selected gait speeds in people post stroke, but other neuromuscular impairments or preferences may drive gait speed even slower than what was predicted to be energy optimal in our simulations. Lastly, our data provide additional theoretical support for the idea that asymmetrical gait patterns may be optimal when aspects of the underlying control system is asymmetrical. Overall, our study is a step towards a better understanding

of how specific impairments in people post-stroke affect gait patterns and metabolic COT. Since it is difficult to study how distributed, unilateral muscle weakness alone affects gait with human participants, our predictive modeling approach can allow for these tests since we can build custom models that represent the type of impairment we are focused on testing. Future studies should extend the work presented here to explore the effects of additional impairments and build a more comprehensive understanding of how a range of impairments influence post-stroke gait.

Acknowledgements

The authors thank Natalia Sánchez for discussions on the content of the paper.

Availability of data and materials

All models and code are available at https://simtk.org/projects/post-stroke-sym

Competing interests

The authors declare that they have no competing interests

Funding

NIH NCMRR R01HD091184

References

1. Gracies JM. Pathophysiology of spastic paresis. II: Emergence of muscle overactivity. Muscle and Nerve. 2005;31(5):552–71.

2. Gracies JM. Pathophysiology of spastic paresis. I: Paresis and soft tissue changes. Muscle and Nerve. 2005;31(5):535–51.

3. Twitchell TE. The restoration of motor function following hemiplegia in man. Brain : a journal of neurology. 1951 Dec;74(4):443–80.

4. Kuo C-L, Hu G-C. Post-stroke Spasticity: A Review of Epidemiology, Pathophysiology, and Treatments. International Journal of Gerontology. 2018 Dec 1;12(4):280–4.

5. Li S. Spasticity, Motor Recovery, and Neural Plasticity after Stroke. Front Neurol. 2017 Apr 3;8:120–120.

6. Neckel N, Pelliccio M, Nichols D, Hidler J. Quantification of functional weakness and abnormal synergy patterns in the lower limb of individuals with chronic stroke. J Neuroeng Rehabil. 2006 Jul 20;3:17.

7. Sánchez N, Acosta AM, López-Rosado R, Dewald JPA. Neural Constraints Affect the Ability to Generate Hip Abduction Torques When Combined With Hip Extension or Ankle Plantarflexion in Chronic Hemiparetic Stroke. Frontiers in Neurology. 2018;9:564.

8. Cruz TH, Dhaher YY. Evidence of abnormal lower-limb torque coupling after stroke: an isometric study. Stroke. 2008 Jan;39(1):139–47.

9. Dewald JP, Pope PS, Given JD, Buchanan TS, Rymer WZ. Abnormal muscle coactivation patterns during isometric torque generation at the elbow and shoulder in hemiparetic subjects. Brain. 1995 Apr;118 (Pt 2):495–510.

10. Sánchez N, Acosta AM, Lopez-Rosado R, Stienen AHA, Dewald JPA. Lower Extremity Motor Impairments in Ambulatory Chronic Hemiparetic Stroke: Evidence for Lower Extremity Weakness and Abnormal Muscle and Joint Torque Coupling Patterns. Neurorehabilitation and neural repair. 2017/08/08 ed. 2017 Sep;31(9):814–26.

11. Finley JM, Bastian AJ. Associations Between Foot Placement Asymmetries and Metabolic Cost of Transport in Hemiparetic Gait. Neurorehabil Neural Repair. 2017 Feb 1;31(2):168–77.

12. Olney SJ, Richards C. Hemiparetic gait following stroke . Part I : Characteristics. Gait and Posture. 1996;4(2):136–48.

13. Perry J, Burnfield J. Gait Analysis: Normal and Pathological Function. Perry J, Burnfield JM, editors. Journal of Sports Science & Medicine. 2010 Jun;9(2):353.

14. Platts MM, Rafferty D, Paul L. Metabolic cost of over ground gait in younger stroke patients and healthy controls. Med Sci Sports Exerc. 2006 Jun;38(6):1041–6.

15. Cruz TH, Lewek MD, Dhaher YY. Biomechanical impairments and gait adaptations post-stroke: multi-factorial associations. Journal of biomechanics. 2009/05/20 ed. 2009 Aug;42(11):1673–7.

16. Hsu A-L, Tang P-F, Jan M-H. Analysis of impairments influencing gait velocity and asymmetry of hemiplegic patients after mild to moderate stroke. Archives of Physical Medicine and Rehabilitation. 2003;84(8):1185–93.

17. Nadeau S, Arsenault AB, Gravel D, Bourbonnais D. Analysis of the clinical factors determining natural and maximal gait speeds in adults with a stroke. Am J Phys Med Rehabil. 1999 Apr;78(2):123–30.

18. Suzuki K, Imada G, Iwaya T, Handa T, Kurogo H. Determinants and predictors of the maximum walking speed during computer-assisted gait training in hemiparetic stroke patients. Arch Phys Med Rehabil. 1999 Feb;80(2):179–82.

19. Ellis RG, Howard KC, Kram R. The metabolic and mechanical costs of step time asymmetry in walking. Proc Biol Sci. 2013 Feb 13;280(1756):20122784–20122784.

20. Stenum J, Choi JT. Disentangling the energetic costs of step time asymmetry and step length asymmetry in human walking. J Exp Biol. 2021 Jun 15;224(12).

21. Nguyen TM, Jackson RW, Aucie Y, de Kam D, Collins SH, Torres-Oviedo G. Self-selected step length asymmetry is not explained by energy cost minimization in individuals with chronic stroke. Journal of NeuroEngineering and Rehabilitation. 2020 Aug 26;17(1):119.

22. Padmanabhan P, Rao KS, Gulhar S, Cherry-Allen KM, Leech KA, Roemmich RT. Persons post-stroke improve step length symmetry by walking asymmetrically. Journal of NeuroEngineering and Rehabilitation. 2020 Aug 3;17(1):105.

23. Roemmich RT, Leech KA, Gonzalez AJ, Bastian AJ. Trading Symmetry for Energy Cost During Walking in Healthy Adults and Persons Poststroke. Neurorehabil Neural Repair. 2019 Aug 1;33(8):602–13.

24. Ryan HP, Husted C, Lewek MD. Improving Spatiotemporal Gait Asymmetry Has Limited Functional Benefit for Individuals Poststroke. Journal of Neurologic Physical Therapy [Internet]. 2020;44(3). Available from:

https://journals.lww.com/jnpt/Fulltext/2020/07000/Improving_Spatiotemporal_Gait_Asymmetry_Has.5.aspx

25. Sánchez N, Finley JM. Individual Differences in Locomotor Function Predict the Capacity to Reduce Asymmetry and Modify the Energetic Cost of Walking Poststroke. Neurorehabil Neural Repair. 2018 Aug 1;32(8):701–13.

26. Falisse A, Serrancolí G, Dembia CL, Gillis J, Jonkers I, De Groote F. Rapid predictive simulations with complex musculoskeletal models suggest that diverse healthy and pathological human gaits can emerge from similar control strategies. Journal of The Royal Society Interface. 2019;16(157):20190402.

27. Song S, Geyer H. Predictive neuromechanical simulations indicate why walking performance declines with ageing. The Journal of physiology. 2018/03/02 ed. 2018 Apr;596(7):1199–210.

28. Ackermann M, van den Bogert AJ. Optimality principles for model-based prediction of human gait. Journal of Biomechanics. 2010 Apr;43(6):1055–60.

29. Anderson FC, Pandy MG. Dynamic optimization of human walking. Journal of Biomechanical Engineering. 2001 Oct;123(5):381–90.

30. Lin Y-C, Walter JP, Pandy MG. Predictive Simulations of Neuromuscular Coordination and Joint-Contact Loading in Human Gait. Annals of Biomedical Engineering. 2018 Aug 1;46(8):1216–27.

31. Miller RH. A comparison of muscle energy models for simulating human walking in three dimensions. Journal of Biomechanics. 2014 Apr;47(6):1373–81.

32. Nguyen VQ, Johnson RT, Sup FC, Umberger BR. Bilevel Optimization for Cost Function Determination in Dynamic Simulation of Human Gait. IEEE Transactions on Neural Systems and Rehabilitation Engineering. 2019 Jul 1;27(7):1426–35.

620 33. Fregly BJ, Reinbolt JA, Rooney KL, Mitchell KH, Chmielewski TL. Design of patient-specific gait
621 modifications for knee osteoarthritis rehabilitation. IEEE Trans Biomed Eng. 2007 Sep;54(9):1687–
622 95.

623 34. Ong CF, Geijtenbeek T, Hicks JL, Delp SL. Predicting gait adaptations due to ankle plantarflexor
624 muscle weakness and contracture using physics-based musculoskeletal simulations. PLoS Comput
625 Biol. 2019 Oct;15(10):e1006993.

626 35. Koelewijn AD, van den Bogert AJ. Joint contact forces can be reduced by improving joint moment
627 symmetry in below-knee amputee gait simulations. Gait Posture. 2016 Sep;49:219–25.

628 36. Miller RH, Brandon SCE, Deluzio KJ. Predicting sagittal plane biomechanics that minimize the
629 axial knee joint contact force during walking. J Biomech Eng. 2013 Jan;135(1):011007.

630 37. Dembia CL, Bianco NA, Falisse A, Hicks JL, Delp SL. OpenSim Moco: Musculoskeletal optimal
631 control. PLOS Computational Biology. 2021 Dec 28;16(12):e1008493.

632 38. Falisse A, Serrancolí G, Dembia CL, Gillis J, De Groote F. Algorithmic differentiation improves the
633 computational efficiency of OpenSim-based trajectory optimization of human movement. PLOS
634 ONE. 2019 Oct 17;14(10):e0217730.

635 39. Nitschke M, Dorschky E, Heinrich D, Schlarb H, Eskofier BM, Koelewijn AD, et al. Efficient
636 trajectory optimization for curved running using a 3D musculoskeletal model with implicit
637 dynamics. Scientific Reports. 2020;10(1):17655.

638 40. De Groote F, Falisse A. Perspective on musculoskeletal modelling and predictive simulations of
639 human movement to assess the neuromechanics of gait. Proc Biol Sci. 2021 Mar
640 10;288(1946):20202432.

641 41. De Groote F, Kinney AL, Rao AV, Fregly BJ. Evaluation of Direct Collocation Optimal Control
642 Problem Formulations for Solving the Muscle Redundancy Problem. Annals of biomedical
643 engineering. 2016 Oct;44(10):2922–36.

644 42. Serrancolí G, Falisse A, Dembia C, Vantilt J, Tanghe K, Lefeber D, et al. Subject-Exoskeleton
645 Contact Model Calibration Leads to Accurate Interaction Force Predictions. IEEE Transactions on
646 Neural Systems and Rehabilitation Engineering. 2019;27(8):1597–605.

647 43. Crowninshield RD, Brand RA. A physiologically based criterion of muscle force prediction in
648 locomotion. Journal of Biomechanics. 1981;

649 44. Bertram JE, Ruina A. Multiple walking speed-frequency relations are predicted by constrained
650 optimization. Journal of theoretical biology. 2001 Apr;209(4):445–53.

651 45. Donelan JM, Kram R, Kuo AD. Mechanical and metabolic determinants of the preferred step width
652 in human walking. Proceedings of the Royal Society B: Biological Sciences. 2001
653 Oct;268(1480):1985–92.

654 46. Kuo AD, Donelan JM. Dynamic Principles of Gait and Their Clinical Implications. Physical
655 Therapy. 2010 Feb;90(2):157–74.

656 47. Ralston HJ. Energy-speed relation and optimal speed during level walking. Internationale Zeitschrift
657 fur angewandte Physiologie, einschliesslich Arbeitsphysiologie. 1958;17(4):277–83.

658 48. Sánchez N, Simha SN, Donelan JM, Finley JM. Using asymmetry to your advantage: learning to
659 acquire and accept external assistance during prolonged split-belt walking. Journal of
660 Neurophysiology. 2021 Feb 1;125(2):344–57.

661 49. Seethapathi N, Srinivasan M. The metabolic cost of changing walking speeds is significant, implies
662 lower optimal speeds for shorter distances, and increases daily energy estimates. Biol Lett. 2015
663 Sep;11(9):20150486.

664 50. Bohannon RW, Andrews AW, Smith MB. Rehabilitation goals of patients with hemiplegia.
665 International Journal of Rehabilitation Research [Internet]. 1988;11(2). Available from:
666 https://journals.lww.com/intjrehabilres/Fulltext/1988/06000/Rehabilitation_goals_of_patients_with_
667 hemiplegia.12.aspx

668 51. Betts JT. Practical Methods for Optimal Control and Estimation Using Nonlinear Programming,
669 Second Edition [Internet]. Society for Industrial and Applied Mathematics; 2010 [cited 2021 Jul
670 29]. 442 p. (Advances in Design and Control). Available from:
671 https://doi.org/10.1137/1.9780898718577

672 52. Andersson JAE, Gillis J, Horn G, Rawlings JB, Diehl M. CasADi: a software framework for
673 nonlinear optimization and optimal control. Mathematical Programming Computation. 2019 Mar
674 1;11(1):1–36.

675 53. Wächter A, Biegler LT. On the implementation of an interior-point filter line-search algorithm for
676 large-scale nonlinear programming. Mathematical Programming. 2006 Mar 1;106(1):25–57.

677 54. Park S, Liu C, Sánchez N, Tilson JK, Mulroy SJ, Finley JM. Using Biofeedback to Reduce Step
678 Length Asymmetry Impairs Dynamic Balance in People Poststroke. Neurorehabil Neural Repair.
679 2021 Jun 1;15459683211019346.

680 55. Umberger BR. Stance and swing phase costs in human walking. Journal of the Royal Society,
681 Interface / the Royal Society. 2010 Sep;7(50):1329–40.

682 56. Umberger BR, Gerritsen KG, Martin PE. A model of human muscle energy expenditure. Computer
683 methods in biomechanics and biomedical engineering. 2003 Apr;6(2):99–111.

684 57. Koelewijn AD, Heinrich D, van den Bogert AJ. Metabolic cost calculations of gait using
685 musculoskeletal energy models, a comparison study. PLOS ONE. 2019 Sep 18;14(9):e0222037.

686 58. Bhargava LJ, Pandy MG, Anderson FC. A phenomenological model for estimating metabolic
687 energy consumption in muscle contraction. Journal of Biomechanics. 2004;37(1):81–8.

688 59. Stoquart G, Detrembleur C, Lejeune T. Effect of speed on kinematic, kinetic, electromyographic
689 and energetic reference values during treadmill walking. Neurophysiologie Clinique/Clinical
690 Neurophysiology. 2008 Apr 1;38(2):105–16.

691 60. Nilsson J, Thorstensson A. Ground reaction forces at different speeds of human walking and
692 running. Acta Physiologica Scandinavica. 1989 Jun;136(2):217–27.

693 61. Margaria R. Positive and negative work performances and their efficiencies in human locomotion.
694 Internationale Zeitschrift fur angewandte Physiologie, einschliesslich Arbeitsphysiologie. 1968
695 May;25(4):339–51.

696 62. Umberger BR, Martin PE. Mechanical power and efficiency of level walking with different stride
697 rates. The Journal of experimental biology. 2007 Sep;210(Pt 18):3255–65.

698 63. Zarrugh MY, Todd FN, Ralston HJ. Optimization of energy expenditure during level walking.
699 European journal of applied physiology and occupational physiology. 1974;33(4):293–306.

700 64. Zarrugh MY, Radcliffe CW. Predicting metabolic cost of level walking. European journal of
701 applied physiology and occupational physiology. 1978 Apr;38(3):215–23.

65. Sánchez N, Schweighofer N, Finley J. Different Biomechanical Variables Explain Within-Subjects Versus Between-Subjects Variance in Step Length Asymmetry Post-Stroke. IEEE Transactions on Neural Systems and Rehabilitation Engineering. 2021;29:1188–98.

66. Roerdink M, Beek PJ. Understanding inconsistent step-length asymmetries across hemiplegic stroke patients: impairments and compensatory gait. Neurorehabil Neural Repair. 2011 Apr;25(3):253–8.

67. Awad LN, Palmer JA, Pohlig RT, Binder-Macleod SA, Reisman DS. Walking speed and step length asymmetry modify the energy cost of walking after stroke. Neurorehabil Neural Repair. 2015 Jun;29(5):416–23.

68. Chen G, Patten C, Kothari DH, Zajac FE. Gait differences between individuals with post-stroke hemiparesis and non-disabled controls at matched speeds. Gait Posture. 2005 Aug;22(1):51–6.

69. Stoquart G, Detrembleur C, Lejeune TM. The reasons why stroke patients expend so much energy to walk slowly. Gait Posture. 2012 Jul;36(3):409–13.

70. Dons B, Bollerup K, Bonde-Petersen F, Hancke S. The effect of weight-lifting exercise related to muscle fiber composition and muscle cross-sectional area in humans. Eur J Appl Physiol Occup Physiol. 1979 Jan 10;40(2):95–106.

71. Miller RH, Hamill J. Optimal footfall patterns for cost minimization in running. Journal of Biomechanics. 2015 Aug 20;48(11):2858–64.

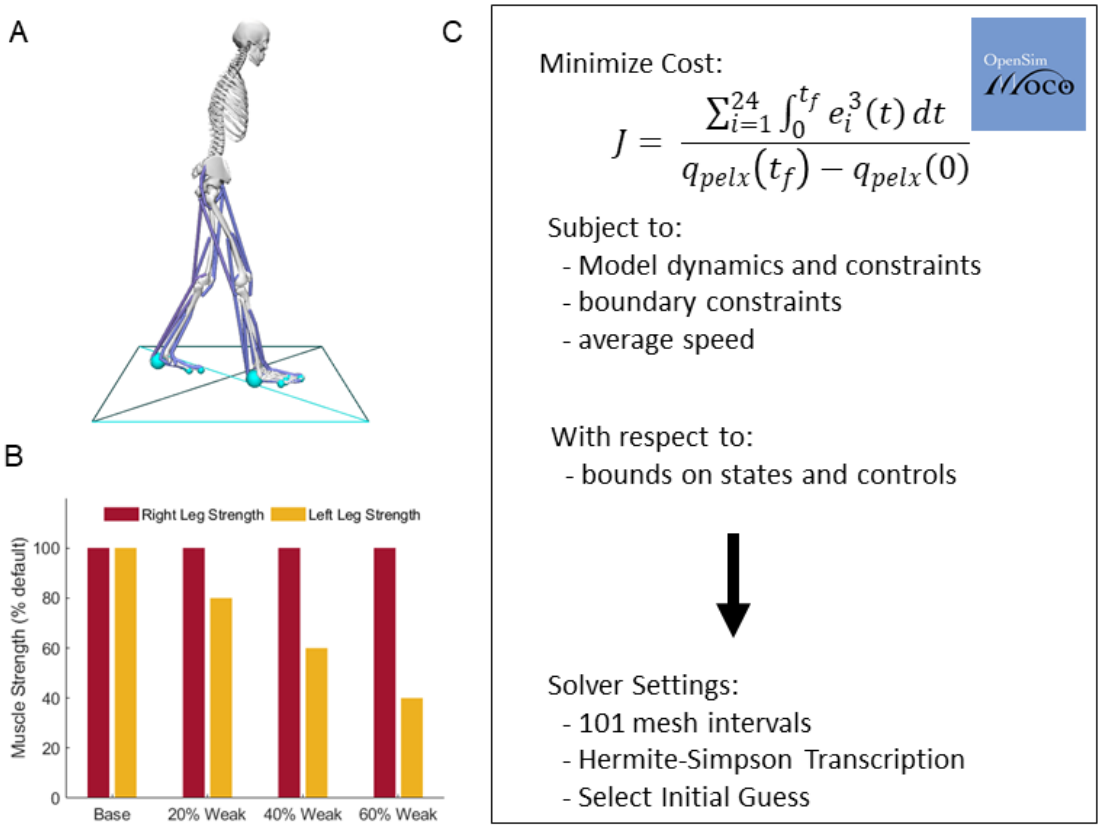

Fig 1: Summary of Set Up. A) Two-dimensional musculoskeletal model with 11 mechanical degrees-of-freedom and 24 muscle-tendon units, B) Maximum isometric muscle forces relative to base model for the 20%, 40% and 60% weak models, muscle strength was uniformly reduced on the left limb, C) Overview of optimization process in Moco adapted from (37), where the objective function (Eqs 1, 5, or 6 respectively from methods) and constraints (Eqs 2 and 3 from methods) for the problem are sent to the solver, with specified settings. Note that the objective function value seen here is for the nominal optimizations, see the methods for further details.

720

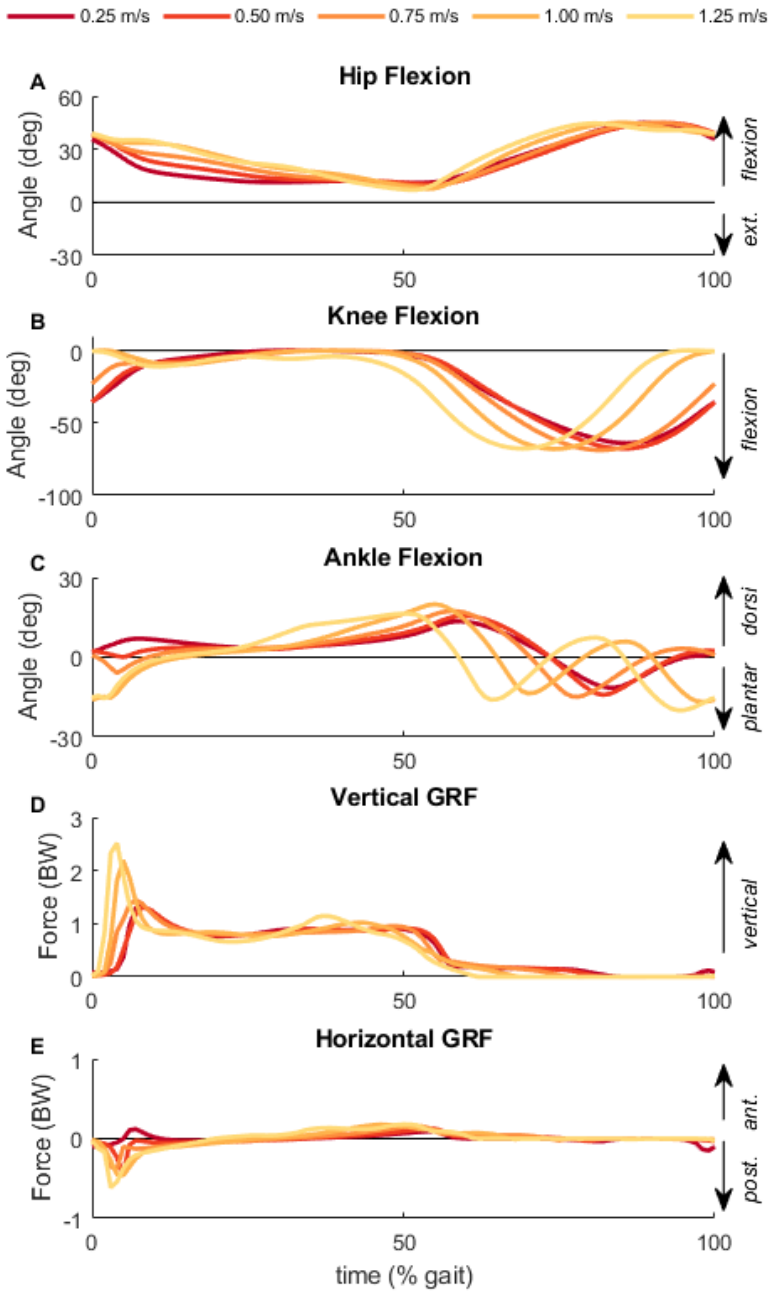

Fig 2: Baseline Kinematic and Ground Reaction Forces. The (A) hip flexion, (B) knee flexion, (C) ankle flexion angles and (D) vertical GRF and (E) horizontal GRF for the base model across each of the five gait speeds. Time is normalized to the gait cycle with 0% being the time of right heel strike.

721

722

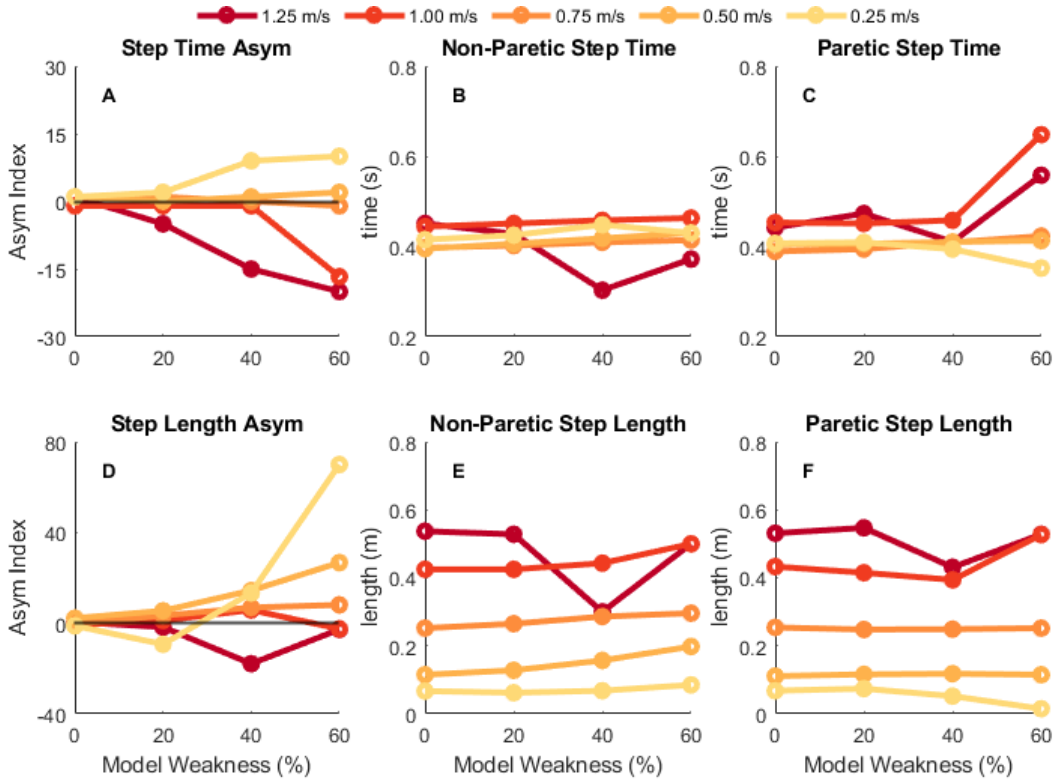

Fig 3: Step time and step length results. Spatiotemporal results for step time (top row) and step length (bottom row) for each condition and each speed. The leftmost column is the step time or step length asymmetry index (A, D), middle column is the non-paretic (right) step time or step length value (B, E), and rightmost column is the paretic (left) step time or step length value (C, F). Darker, red colors depict results for faster speeds while lighter, yellow colors depict results for slower speeds. Positive asymmetry indices indicate that the non-paretic value is greater than the paretic value, whereas negative asymmetry indices indicate that the paretic value is greater than the non-paretic value.

723

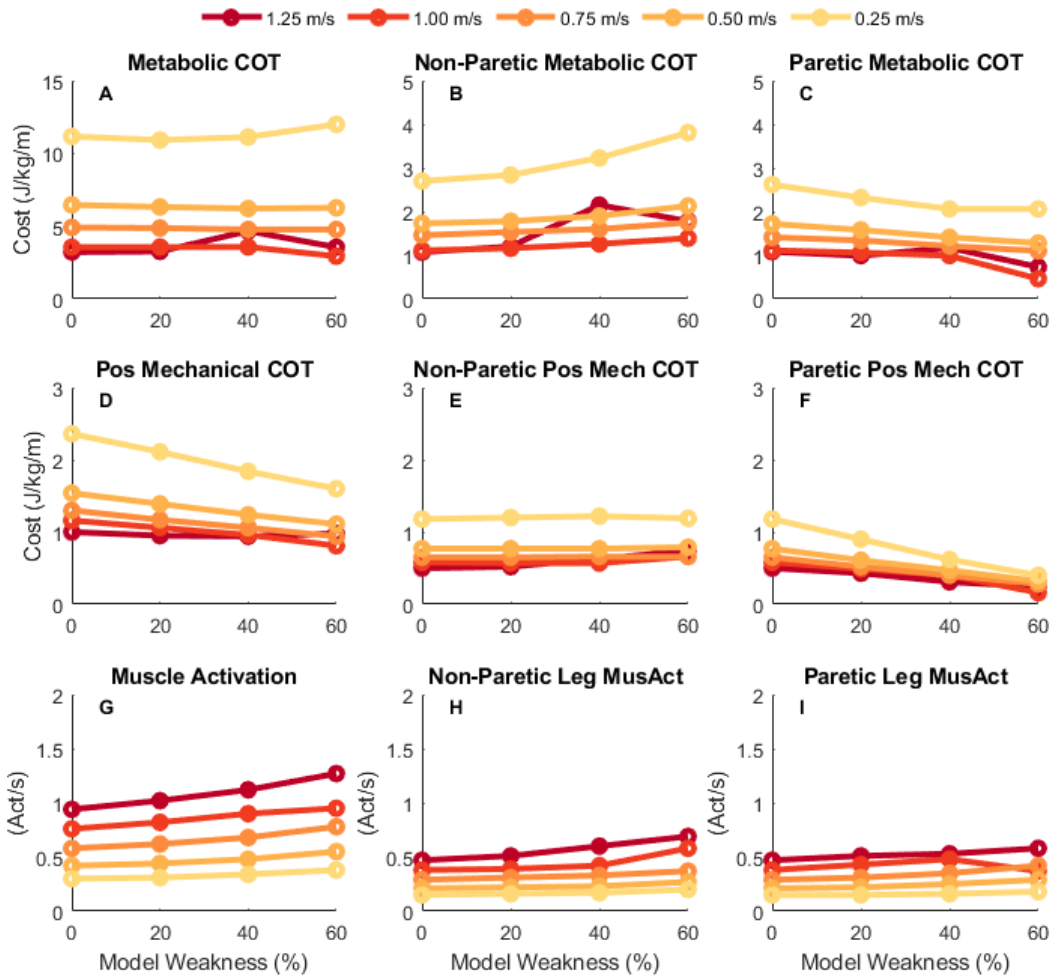

Fig 4: Metabolic and Mechanical Cost of Transport. Metabolic cost of transport (COT; top row), positive mechanical COT (middle row), and sum of the integrated muscle activation (bottom row) for each condition. The leftmost column shows the result for the sum across both limbs, while the middle column shows the results for the non-paretic (right) limb and the rightmost column shows the result for the paretic (left) limb. Darker, red colors are for faster speeds while lighter, yellow colors are for slower speeds. Metabolic COT remained relatively consistent within a speed across the different weakness models, partially a result of an increase in mechanical work done by the right (non-paretic) limb with a proportional decrease in mechanical work done by the left (paretic) limb.

724

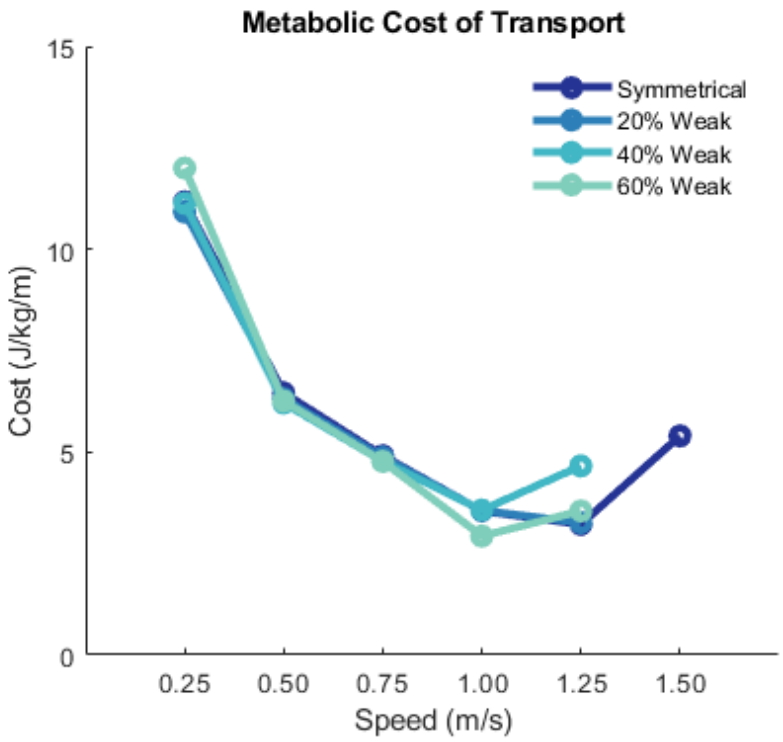

Fig 5: Metabolic cost of transport across speeds. Dark blue represents results for the symmetrical (or base) model, while blue-green lighter colors represent the asymmetrical models. The symmetrical condition included an optimization at 1.50 m/s so that we could establish the U-shaped curve of metabolic cost (where 1.25 is approximately the metabolic-optimal speed for the symmetrical model). We did not solve the optimal control problem for other models at 1.50 m/s because the weakness in the 40% and 60% models prevented convergence at speeds faster that 1.25 m/s.

725

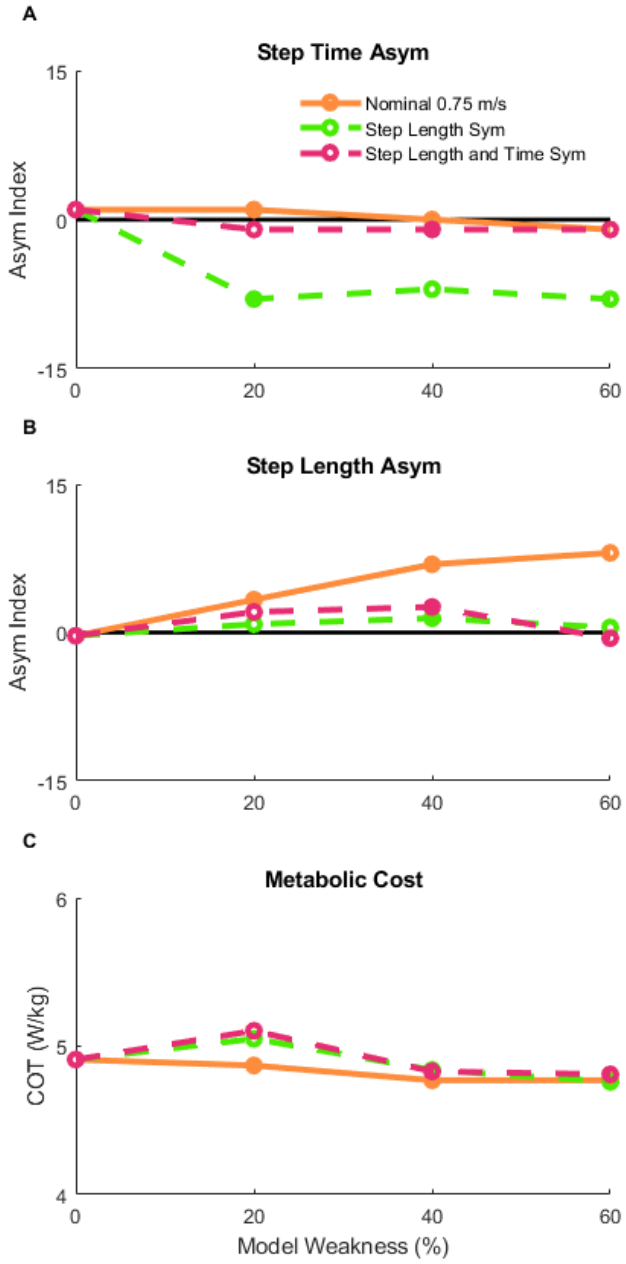

Fig 6: Secondary Analysis of Spatiotemporal asymmetry. After the nominal conditions (orange solid line), additional optimizations were performed across the three hemiparetic models with the goal of reducing the step length asymmetry (green dashed line) to assess the effect of enforced step length (B) symmetry on step time asymmetry (A) and metabolic cost (C). Finally, a set of optimizations were performed with the goal of reducing both step length and step time asymmetry (purple dashed line).